


Monitoring early response to chemoradiotherapy with ^{18}F -FMISO dynamic PET in head and neck cancer

Milan Grkovski¹  · Nancy Y. Lee² · Heiko Schöder³ · Sean D. Carlin³ · Bradley J. Beattie¹ · Nadeem Riaz² · Jonathan E. Leeman² · Joseph A. O'Donoghue¹ · John L. Humm¹

Received: 21 February 2017 / Accepted: 3 May 2017 / Published online: 24 May 2017
© Springer-Verlag Berlin Heidelberg 2017

Abstract

Purpose There is growing recognition that biologic features of the tumor microenvironment affect the response to cancer therapies and the outcome of cancer patients. In head and neck cancer (HNC) one such feature is hypoxia. We investigated the utility of ^{18}F -fluoromisonidazole (FMISO) dynamic positron emission tomography (dPET) for monitoring the early microenvironmental response to chemoradiotherapy in HNC. **Experimental design** Seventy-two HNC patients underwent FMISO dPET scans in a customized immobilization mask (0–30 min dynamic acquisition, followed by 10 min static acquisitions starting at ~95 min and ~160 min post-injection) at baseline and early into treatment where patients have already received one cycle of chemotherapy and anywhere from five to ten fractions of 2 Gy per fraction radiation therapy. Voxelwise pharmacokinetic modeling was conducted using an irreversible one-plasma two-tissue compartment model to calculate surrogate biomarkers of tumor hypoxia (k_3 and Tumor-to-Blood Ratio (TBR)), perfusion (K_1) and FMISO distribution volume (DV). Additionally, Tumor-to-Muscle

Ratios (TMR) were derived by visual inspection by an experienced nuclear medicine physician, with $TMR > 1.2$ defining hypoxia.

Results One hundred and thirty-five lesions in total were analyzed. TBR , k_3 and DV decreased on early response scans, while no significant change was observed for K_1 . The k_3 - TBR correlation decreased substantially from baseline scans (Pearson's $r = 0.72$ and 0.76 for mean intratumor and pooled voxelwise values, respectively) to early response scans (Pearson's $r = 0.39$ and 0.40 , respectively). Both concordant and discordant examples of changes in intratumor k_3 and TBR were identified; the latter partially mediated by the change in DV . In 13 normoxic patients according to visual analysis (all having lesions with $TMR = 1.2$), subvolumes were identified where k_3 indicated the presence of hypoxia.

Conclusion Pharmacokinetic modeling of FMISO dynamic PET reveals a more detailed characterization of the tumor microenvironment and assessment of response to chemoradiotherapy in HNC patients than a single static image does. In a clinical trial where absence of hypoxia in primary tumor and lymph nodes would lead to de-escalation of therapy, the observed disagreement between visual analysis and pharmacokinetic modeling results would have affected patient management in <20% cases. While simple static PET imaging is easily implemented for clinical trials, the clinical applicability of pharmacokinetic modeling remains to be investigated.

Electronic supplementary material The online version of this article (doi:10.1007/s00259-017-3720-6) contains supplementary material, which is available to authorized users.

✉ Milan Grkovski
grkovskm@mkscc.org

Keywords Treatment response · ^{18}F -FMISO · Hypoxia · Dynamic PET · Head and neck cancer

¹ Department of Medical Physics, Memorial Sloan Kettering Cancer Center, 1275 York Avenue, New York, NY 10065, USA

² Department of Radiation Oncology, Memorial Sloan Kettering Cancer Center, New York, NY, USA

³ Department of Radiology, Memorial Sloan Kettering Cancer Center, New York, NY, USA

Introduction

There is growing interest in studying essential biologic features of cancer, such as metabolism, hypoxia, and expression

of transmembrane receptors, noninvasively and repeatedly, during therapy. In parallel, efforts are underway to adapt therapies based on early treatment response reflecting cancer biology rather than simple structural changes (e.g., changes in tumor volume or shape). Such biologic changes may be a crucial component in the effective management of many cancer patients [1–5]. An improved understanding of biologic processes and their relationship to functional imaging data and tumor response may yield pertinent information that can be applied in a rational way, such as adaptive radiotherapy [6], patient stratification in clinical trials (e.g., utilizing hypoxia-activated prodrugs; [7]), development of novel pharmaceutical drugs [8] or optimization of treatments utilizing combinations of targeted drugs with radiotherapy [9].

Hypoxia is a common feature of solid tumors and a major negative prognostic indicator regarding patient outcome after radiotherapy [10]. A meta-analysis of clinical trials in patients with head and neck cancer (HNC) undergoing radiotherapy with curative intent concluded that there is evidence in favor of targeting hypoxia through various treatment modifications [11], although discordant results have also been reported [12]. Hypoxic modification continues to have a limited impact on clinical practice, likely due to the non-selectivity of patients entered on clinical trials [13].

Positron emission tomography (PET) using hypoxia selective imaging probes has the ability to detect tumor hypoxia non-invasively. PET imaging with ^{18}F -fluoromisonidazole (FMISO), the most extensively studied hypoxia PET radiotracer, has been shown to be clinically feasible [14, 15] and reproducible [16, 17]. However, Tumor-to-Blood Ratio (*TBR*) or Tumor-to-Muscle Ratio (*TMR*), metrics derived from static FMISO acquisitions that are commonly used as surrogate biomarkers of tumor hypoxia, depend on the exact time point at which images are obtained; in addition, *TBR* and *TMR* also depend on the FMISO distribution volume that is non-uniform both within and between tumors [18]. Therefore, presence and extent of hypoxia may be over- or underestimated with this approach. A method that allows for more accurate quantification of hypoxia may help to improve confidence in interpreting hypoxia PET imaging data, in particular if the presence of hypoxia, and changes in hypoxia under treatment, are to be used to guide patient management.

Pharmacokinetic modeling of FMISO dynamic PET (dPET) in principle enables the derivation of a surrogate biomarker that more directly reflects hypoxia-mediated entrapment, while simultaneously providing information on tumor perfusion that may be important in distinguishing different tumor subtypes [19]. Tumor perfusion is an important measure of drug delivery, and changes in perfusion may provide an insight into the response to either nonspecific or targeted (e.g., antiangiogenic) therapies [20]. We recently demonstrated that simultaneous, multiparametric and single modality imaging of tumor hypoxia and perfusion with FMISO dPET can

be performed in HNC patients with acquisition protocols with overall scan times as low as 20 min, comparable in duration to diagnostic ^{18}F -Fluorodeoxyglucose (FDG) PET [18].

Complex relationships between tumor hypoxia, perfusion and glucose metabolism support the use of composite metrics providing additional information on tumor biology that may help in designing adaptive therapies [8, 21] and may result in better prediction of patient survival [22, 23]. Of note, these characteristics of the tumor microenvironment may not change in a uniform manner under therapy [8].

In the present study, tumor hypoxia, perfusion and FMISO distribution volume were assessed simultaneously from FMISO dPET scans in 72 head and neck cancer patients at baseline and after one cycle of chemotherapy concurrent with anywhere from five to ten fractions of 2 Gy radiation (early response). We hypothesized that pharmacokinetic modeling of FMISO dPET may enable a more comprehensive assessment of tumor response than can be obtained from single static images.

Materials and methods

Patient selection

Patients with HNC were enrolled prospectively to Institutional Review Board approved multi-arm trial (Protocol #04-070Protocol, NCT00606294 on www.clinicaltrials.gov; inclusion criteria: 18+ age, histologically confirmed diagnosis of squamous cell carcinoma of the head and neck, Karnofsky performance status of ≥ 70 ; exclusion criteria: all nasopharyngeal, paranasal sinus, salivary cancer and thyroid malignancies, prior chemotherapy or radiotherapy within the last three years, previous surgical resection for the same disease, any prior radiotherapy to the head and neck region, and pregnancy). All patients signed a written informed consent regarding the examination and use of anonymous data for research and publication purposes. This article reports the results of a small sub-study of the currently ongoing trial (72 patients, aged 60 ± 11 years (range, 25–86 years); Table 1). Flowchart of patient selection and inclusion is presented in Fig. 1.

PET/CT image acquisition and analysis

All patients underwent baseline FDG PET/CT scans of the head and neck for radiotherapy planning purposes, followed after 8 ± 6 days by a baseline FMISO dynamic PET/CT scans (FMISO1). A second FMISO scan (FMISO2) was acquired at 17 ± 5 days after FMISO1, after patients have already received one cycle of chemotherapy and anywhere from five to ten fractions of 2 Gy per fraction radiation therapy. For all scans, patients were positioned on a flat-top couch wearing a

Table 1 Subject demographics and clinical characteristics

	<i>N</i> = 72 (%)
Gender	
Male	66 (92)
Female	6 (8)
Age at diagnosis, y	
< 40	1 (1)
40–49	10 (14)
50–59	30 (42)
60–69	20 (28)
70–79	6 (8)
80+	5 (7)
Clinical tumor classification	
T1	16 (22)
T2	36 (50)
T3	10 (14)
T4	8 (11)
Unknown	2 (3)
Tumor subsite	
Base of tongue	39 (54)
Tonsil	28 (39)
Hypopharynx	1 (1)
Supraglottic larynx	2 (3)
Unknown primary	2 (3)
Clinical lymph node classification	
N1	7 (10)*
N2a	7 (10)
N2b	31 (43)
N2c	25 (35)
N3	2 (3)
HPV status	
Positive	47 (85)
Negative	8 (15)
Testing not performed	17
p16 status	
Positive	5 (8)
Negative	60 (92)
Testing not performed	7
Chemotherapy regimen	
Carboplatin/5-fluorouracil	3 (4)*
Carboplatin/paclitaxel	3 (4)
Cetuximab/cisplatin/bevacizumab/	1 (1)
Cetuximab	7 (10)
Cisplatin	55 (76)
Cisplatin/paclitaxel	1 (1)
Not received	2 (3)

*Numbers do not total 100% due to rounding.

customized radiotherapy treatment immobilization mask that minimizes motion and allows for accurate repositioning.

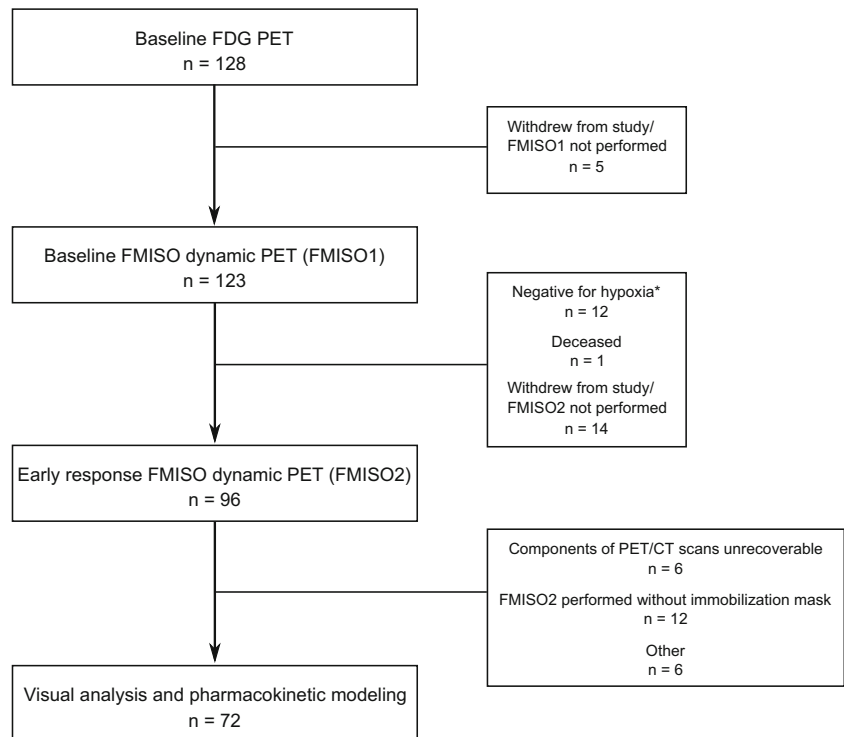
Intravenous lines inserted in antecubital veins were used for radiotracer injection. Patients were administered an intravenous bolus injection of 390 ± 14 MBq of FMISO. Each FMISO dynamic PET acquisition consisted of three segments: (1) at time $t = 0$, a 30 min acquisition binned into 6×5 -s, 3×10 -s, 4×60 -s, 2×150 -s, 2×300 -s and 1×600 -s frames, (2) a 10 min static acquisition, starting at 93 ± 6 min (FMISO1) and 96 ± 9 min (FMISO2) and (3) a 10 min static acquisition starting at 160 ± 13 min (FMISO1) and 161 ± 13 min (FMISO2) post-injection.

For both FMISO1 and FMISO2, all three FMISO segments were spatially co-registered using the rigid-body transformation calculated with General Co-Registration™ tool (General Electric Advantage Workstation v4.7) applied to their corresponding CT scans, and subsequently merged to form a concatenated FMISO dPET scan. These two scan series were also co-registered with the FDG PET scan. Lesions were delineated on the FDG PET images, using the adaptive threshold algorithm in the PET VCAR™ (Volume Computer Assisted Reading; General Electric Advantage Workstation v4.7).

Additionally, Tumor-to-Muscle Ratios (*TMR*) for both FMISO1 and FMISO2 were derived by visual inspection of the three FMISO segments by an experienced nuclear medicine physician (H.S.) as reported previously [6], independently of the medical physicist's (M.G.) pharmacokinetic modeling. Spherical regions of interest were placed in tumors and metastatic lymph nodes, and activity concentration was measured using max SUV in the tumor volume of interest (VOI). Reference regions were placed in contralateral neck muscles showing low background activity and measured using mean SUV. Hypoxia-positive was defined as FMISO uptake in known sites of disease that was increasing or stable from scan time point 1) to time point 3) of each scan series, with a $TMR > 1.2$. Since TBR_{max} was defined similarly (max SUV in the tumor VOI divided by mean SUV in the jugular vein VOI), synchronization of delineation methods was not required.

Pharmacokinetic modeling

Voxelwise pharmacokinetic modeling of FMISO dPET images was performed in PMOD v3.604 (PMOD Technologies GmbH), utilizing an irreversible one-plasma two-tissue compartment model [18]. The output of the pharmacokinetic modeling are three kinetic rate constants: K_1 , the kinetic rate constant describing transport from the vascular compartment to the extravascular tissue compartment and a surrogate biomarker of tumor perfusion, k_2 , the kinetic rate constant describing the transport of FMISO from the extravascular tissue compartment back to blood and k_3 , the kinetic rate constant approximating the rate of irreversible binding of FMISO and a surrogate for hypoxia-mediated entrapment.

Fig. 1 Flowchart of patient selection and inclusion

An important composite parameter DV (distribution volume) is given by

$$DV = v_B + (1 - v_B) \frac{K_1}{k_2} \quad (1)$$

where v_B is the fractional vascular volume also calculated by the model. DV represents the total FMISO distribution volume, i.e., overall concentration of unbound FMISO relative to blood, and sets the threshold above which FMISO accumulation is due to hypoxia specific binding. DV was previously shown to be non-uniform across a tumor upon tracer equilibration [18]. The input function (IF) was delineated on ipsilateral (with respect to the lesion) jugular vein on the early dynamic frame with the highest image intensity, by selecting ~100 hottest voxels. TBR was calculated from the 3rd FMISO acquisition, using the measured activity concentration in the IF volume of interest, $C_p(t)$ as the reference,

$$TBR = \frac{C_{\text{target}}(t)}{C_p(t)} \quad (2)$$

The parameters v_B and DV are unitless, whereas K_1 (assuming unit density tissue), k_2 and k_3 are expressed in units of min^{-1} .

Pharmacokinetic modeling was also performed for ipsilateral (with respect to the primary lesion) sternocleidomastoid muscle, adipose tissue posterior to the cervical vertebrae and ipsilateral submandibular and parotid glands, on both baseline and early response scans.

Statistical analysis

All correlations were performed using Pearson's correlation coefficient r (measure of correlation strength). Linear regression was performed to model the relationship between TBR (dependent variable) and k_3 (explanatory variable), and to calculate the slope coefficient (measure of correlation direction) and intercept coefficient. Comparisons of investigated metrics as calculated from (1) baseline and early response scans or (2) primary lesions and lymph nodes were performed with unpaired 2-tailed Student t test. A $p < 0.05$ was assumed to represent statistical significance.

Results

In total, 135 lesions were analyzed (54 primaries and 81 lymph nodes) by both pharmacokinetic modeling and, independently, by visual analysis. The results of these analyses were subsequently compared side by side by a nuclear medicine physician, nuclear medicine physicists and the radiation oncologists. The lesions ranged from 2 to 54 cm^3 (median volume: 10 cm^3). HPV (by in situ hybridization) and p16 testing (by immunohistochemistry) was performed in 56 and 64 patients, respectively, with 84% and 92% of tested patients harboring HPV positive and p16 positive tumors, respectively. Four out of 72 patients were deceased at the time of writing, while an additional two patients experienced local disease

relapse (median follow-up period: 26 months, range: 5–73 months).

Mean values determined for all investigated parameters (i.e., TBR , k_3 , DV , K_1 and v_B) as well as means from voxelwise analysis of pooled data are summarized in Table 2. Changes between early response and baseline FMISO scan data are displayed in Fig. 2 for TBR , k_3 , DV , K_1 and v_B . There is a visible shift to reduced values for both TBR and k_3 , indicative of a decrease in hypoxia early during treatment. Baseline k_3 was the only metric that was significantly different between primaries and lymph nodes (Supplementary Table S1).

Corresponding values for normal tissues in the head and neck region are presented in Table 3. Apart from a small but significant decrease in TBR and DV values in submandibular gland, none of the investigated parameters were significantly different between baseline and early response scans for any of analyzed normal tissues.

Pearson's r between mean voxelwise k_3 and TBR in baseline scans was 0.72 (95% CI: 0.63–0.79; Fig. 3a). Each point in Fig. 3a is color-coded according to the mean DV for that tumor, illustrating that non-uniformity in the tumor DV reduces the k_3 - TBR correlation over the patient population as a whole. These analyses were also performed on a voxel-by-voxel basis for the entire voxel data ensemble from all tumors. The results are displayed as an intensity histogram for the pooled voxelwise k_3 - TBR data with the regression line ($r = 0.76$; Fig. 3b). Lower correlation between k_3 and TBR was observed in the results from early response scans, both on intratumor ($r = 0.39$, 95% CI: 0.24–0.53; Fig. 3c) and voxelwise ($r = 0.40$; Fig. 3d) levels. The change in mean intratumor k_3 ($\Delta k_3 = k_{3,FMISO2} - k_{3,FMISO1}$) positively correlated with the change in mean intratumor TBR ($\Delta TBR = TBR_{FMISO2} - TBR_{FMISO1}$; $r = 0.70$, $p < 0.01$; Supplementary Figure S1A). Additionally, Δk_3 negatively correlated with the change in mean intratumor DV ($\Delta DV = DV_{FMISO2} - DV_{FMISO1}$; $r = -0.56$, $p < 0.01$; Supplementary Figure S1B). The correlations between metrics as calculated from baseline and early response scans were: $r(TBR_{FMISO1}, TBR_{FMISO2}) = 0.58$, $r(k_{3,FMISO1}, k_{3,FMISO2}) = 0.41$, $r(DV_{FMISO1}, DV_{FMISO2}) = 0.53$, $r(K_{1,FMISO1}, K_{1,FMISO2}) = 0.41$ and

$r(v_{B,FMISO1}, v_{B,FMISO2}) = 0.39$ ($p < 0.01$ in all cases). The correlations between metrics as calculated from baseline scans and their change after early response scans were $r(TBR_{FMISO1}, \Delta TBR) = -0.90$, $r(k_{3,FMISO1}, \Delta k_3) = -0.75$, $r(DV_{FMISO1}, \Delta DV) = -0.53$, $r(K_{1,FMISO1}, \Delta K_1) = -0.43$ and $r(v_{B,FMISO1}, \Delta v_B) = -0.48$ ($p < 0.01$ in all cases).

Pharmacokinetic modeling facilitated a more detailed early response assessment to chemoradiotherapy. This is best revealed by investigating individual patient cases that highlight the diversity of individual responses. The parametric maps for two patients reveal a concordance (Fig. 4a) and discordance (Fig. 4b) in changes in TBR and k_3 , two surrogate metrics of tumor hypoxia derived from static and dynamic PET scans, respectively. For patient #1, the decrease in k_3 ($\Delta k_3 = -0.0066 \text{ min}^{-1}$) was reflected in the decrease in TBR ($\Delta TBR = -1.26$), with no discernible change in DV (Fig. 4a). However, for patient #2 (Fig. 4b), the decrease in TBR ($\Delta TBR = -0.17$) and DV ($\Delta DV = -0.24$) was observed, whereas k_3 increased ($\Delta k_3 = 0.0026 \text{ min}^{-1}$).

TMR readings for both baseline and early response FMISO scans were available for 129 out of 135 lesions (for the remaining six lesions, TMR readings were not made on early response scans due to indiscernible FMISO uptake, thus assuming the resolution of hypoxia). Pearson's r between TBR_{max} (derived as part of pharmacokinetic modeling) and TMR (derived independently by a nuclear medicine physician) was 0.94 and 0.84 on baseline and early response scans, respectively. However, Pearson's r between $k_{3,max}$ and TMR was 0.66 and 0.33 on baseline and early response scans, respectively.

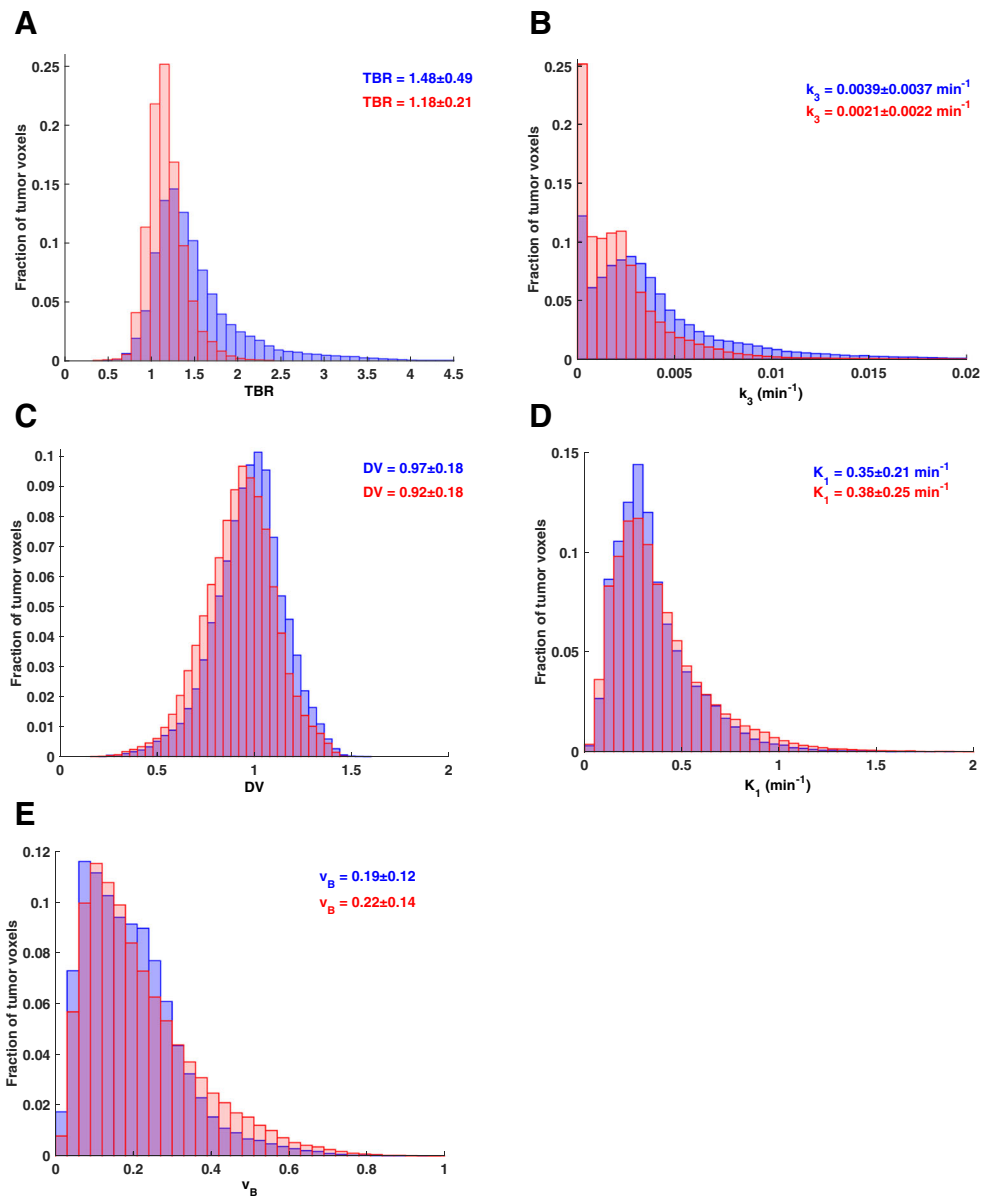
On baseline scans, TMR was ≤ 1.2 in 22 lesions, suggesting absence of hypoxia, with 18 out of these 22 lesions having $TMR \leq 1.2$ also on early response scans (in the remaining four lesions, TMR increased to 1.3). $TMR \leq 1.2$ was observed in 56 lesions on early response scans (included are lesions for which FMISO uptake was indiscernible). In 21 out of these 56 lesions (eight primaries and 13 lymph nodes), 4+ consecutive voxels with $k_3 \geq 0.0026 \text{ min}^{-1}$ were identified on early response scans, suggesting the presence of some hypoxia by pharmacokinetic modeling. The k_3 threshold was derived as mean $k_3 + 3$ standard deviations of the value as measured in

Table 2 Summary of investigated metrics for the baseline and early response FMISO dynamic PET scans in tumors ($n = 135$)

	Tumor-to-blood Ratio	k_3 (min^{-1})	Distribution volume	K_1 (min^{-1})	v_B
Baseline (mean intratumor)	1.35 \pm 0.31	0.0029 \pm 0.0022	0.97 \pm 0.14	0.38 \pm 0.17	0.20 \pm 0.10
Early response (mean intratumor)	1.12 \pm 0.15	0.0020 \pm 0.0016	0.91 \pm 0.14	0.41 \pm 0.21	0.21 \pm 0.11
p -value*	<0.01	<0.01	<0.01	0.20	0.28
Mean difference	-0.22 \pm 0.26	-0.0009 \pm 0.0021	-0.06 \pm 0.14	0.03 \pm 0.21	0.01 \pm 0.12
Baseline (voxelwise)	1.48 \pm 0.49	0.0039 \pm 0.0037	0.97 \pm 0.18	0.35 \pm 0.21	0.19 \pm 0.12
Early response (voxelwise)	1.18 \pm 0.21	0.0021 \pm 0.0022	0.92 \pm 0.18	0.38 \pm 0.25	0.22 \pm 0.14

*Unpaired 2-tailed Student t test.

Fig. 2 Voxelwise distributions of investigated parameters derived from baseline and early response FMISO dynamic PET scans. **a** Normalized distribution histogram of voxelwise *TBR* values at baseline (blue) and after one cycle of chemoradiotherapy (red), derived from pooled data. **b** Equivalent histogram for k_3 . **c** Equivalent histogram for *DV*. **d** Equivalent histogram for K_1 . **e** Equivalent histogram for v_B



non-diseased sternocleidomastoid muscle on both baseline and early response scans. In all cases, the tumor region with highest k_3 also exhibited the lowest *DV*, typically between 0.4 and 0.6 (thus causing underestimation of total FMISO uptake), possibly indicating a mixture of severely hypoxic, cystic and/or partially necrotic tissue. In 14 lesions, *TMR* > 1.2 was observed on early response scans whereas k_3 was <0.0026 min⁻¹ throughout the lesion.

Patient-based results are summarized in Table 4. The majority of patients (69 out of 72) were hypoxia-positive (i.e., having at least one lesion with *TMR* > 1.2) on baseline scans. The normoxic three patients remained hypoxia-negative on early response scans, while hypoxia resolution was observed in 20 out of the previously hypoxic 69 patients. In 13 patients without *TMR* > 1.2 lesions on early response scans,

pharmacokinetic modeling indicated the presence of hypoxic regions. However, all 13 of these patients had at least one lesion with *TMR* = 1.2. In five patients, *TMR* > 1.2 was observed on early response scans, whereas k_3 was <0.0026 min⁻¹ throughout all patients' lesions.

Discussion

Monitoring early treatment response by imaging studies may provide information that can be used to design response-adapted therapy strategies. However, it is imperative that the therapy-induced changes be interpreted correctly. Establishing a non-invasive and quantitative measurement of the tumor hypoxic burden is an important first step in testing the clinical

Table 3 Summary of investigated metrics for the baseline and early response FMISO dynamic PET scans in normal tissues ($n = 72$ patients)

		Target-to-blood Ratio	k_3 (min^{-1})	Distribution volume	K_1 (min^{-1})	v_B
Sternocleidomastoid muscle	Baseline	1.01 ± 0.08	0.0007 ± 0.0006	0.89 ± 0.10	0.08 ± 0.04	0.05 ± 0.03
	Early response	1.00 ± 0.09	0.0008 ± 0.0007	0.89 ± 0.12	0.09 ± 0.04	0.06 ± 0.04
	p -value*	0.46	0.78	0.98	0.24	0.13
	Mean difference	-0.01 ± 0.09	0.0000 ± 0.0007	0.00 ± 0.07	0.01 ± 0.05	0.01 ± 0.04
Adipose tissue	Baseline	0.27 ± 0.07	0.0004 ± 0.0004	0.24 ± 0.06	0.02 ± 0.01	0.01 ± 0.01
	Early response	0.25 ± 0.07	0.0004 ± 0.0005	0.23 ± 0.06	0.02 ± 0.02	0.01 ± 0.01
	p -value*	0.11	0.69	0.40	0.85	0.84
	Mean difference	-0.02 ± 0.05	0.0000 ± 0.0006	-0.01 ± 0.05	0.00 ± 0.02	0.00 ± 0.01
Submandibular gland	Baseline	1.02 ± 0.08	0.0002 ± 0.0003	1.04 ± 0.11	0.74 ± 0.53	0.16 ± 0.10
	Early response	1.00 ± 0.09	0.0003 ± 0.0004	0.98 ± 0.10	0.76 ± 0.40	0.18 ± 0.11
	p -value*	0.03	0.19	<0.01	0.86	0.30
	Mean difference	-0.03 ± 0.08	0.0001 ± 0.0005	-0.06 ± 0.10	0.01 ± 0.55	0.02 ± 0.13
Parotid gland	Baseline	0.90 ± 0.11	0.0002 ± 0.0004	0.88 ± 0.15	0.50 ± 0.32	0.10 ± 0.08
	Early response	0.87 ± 0.11	0.0003 ± 0.0005	0.84 ± 0.11	0.56 ± 0.32	0.12 ± 0.09
	p -value*	0.13	0.17	0.09	0.35	0.37
	Mean difference	-0.03 ± 0.09	0.0001 ± 0.0006	-0.04 ± 0.10	0.05 ± 0.32	0.01 ± 0.10

*Unpaired 2-tailed Student t test.

relevance of hypoxia and its utility as a tumor response biomarker. While the association between pre-treatment tumor hypoxia and poor overall survival after radiotherapy has been reviewed previously [10], recent reports also suggest that FMISO imaging during the initial phase of treatment carries prognostic value for identifying HNC patients at risk from local recurrence [24, 25]. In the current study, we performed baseline and early response FMISO dynamic PET scans in 72 HNC patients to assess the added value of pharmacokinetic modeling for elucidating changes in tumor hypoxia after initiation of chemoradiotherapy.

Static metrics of FMISO images rely on the implicit assumption that FMISO distribution volume (DV) is close to unity in all tissues with dispersion not greater than what can be attributed to image noise. While we have found that DV is indeed close to 1.0 in normal non-adipose tissues in the head and neck region, including sternocleidomastoid muscle and large salivary glands, DV was observed to be non-uniform with a relatively wide spread around 1 within tumor lesions, resulting in an over- or underestimation of the tumor hypoxic fraction [18]. In adipose tissue, the DV was found to be ~ 0.25 (reflecting the octanol-water partition coefficient of ~ 0.4). The dependence of DV on tissue composition may potentially explain low intratumor DV values resulting from heterogeneous stroma that contains adipose-like tissue and partially necrotic areas with dysfunctional vasculature. Lesions with DV values greater than 1.0 were also identified (Fig. 4b), suggesting a non-specific mechanism of radiotracer accretion.

Calculation of k_3 (a time independent kinetic rate constant) from pharmacokinetic modeling of dynamic PET data results in a more direct surrogate for hypoxia-mediated entrapment

than the FMISO uptake from a static scan, since the estimation of k_3 is independent of DV , tumor perfusion and imaging time post-injection. In general, changes in TBR and k_3 on a whole tumor level were well correlated. However, in 18 out of 148 lesions, the total intratumor FMISO uptake decreased on the early response scan ($\Delta TBR \leq -0.10$) while the hypoxia parameter k_3 remained unchanged or increased ($\Delta k_3 \geq 0.0000 \text{ min}^{-1}$), in part because of a decrease in DV ($\Delta DV = -0.22 \pm 0.12$). The correlation between k_3 and TBR was lower on early response scans compared to baseline scans, indicating the importance of also accounting for the changes in DV when interpreting FMISO static uptake. The changes in DV might be secondary to radiation-induced alteration of the soluble and insoluble components of the tumor microenvironment that affects tissue composition (e.g., leading to the development of cystic structures or necrosis; [26]). The early response scans also result in a convergence of TBR values to values around 1.0 and an increase in the number of operationally zero k_3 values, a possible and expected consequence of radiation-induced reoxygenation [27]. FMISO2 scans were performed relatively early into treatment, after patients received one cycle of chemotherapy and 5–10 fractions of 2Gy/fraction radiotherapy. We observed that, in general, tumor shrinkage lagged behind functional change. In a recent study in a same cohort of HNC patients, Paudyal et al. reported an increase in the apparent diffusion coefficient on diffusion-weighted MRI, indicating a decrease in cellularity in the tumors weeks before any observed volume reduction [28].

The patient examples highlight the potential of FMISO pharmacokinetic modeling to elucidate microenvironmental

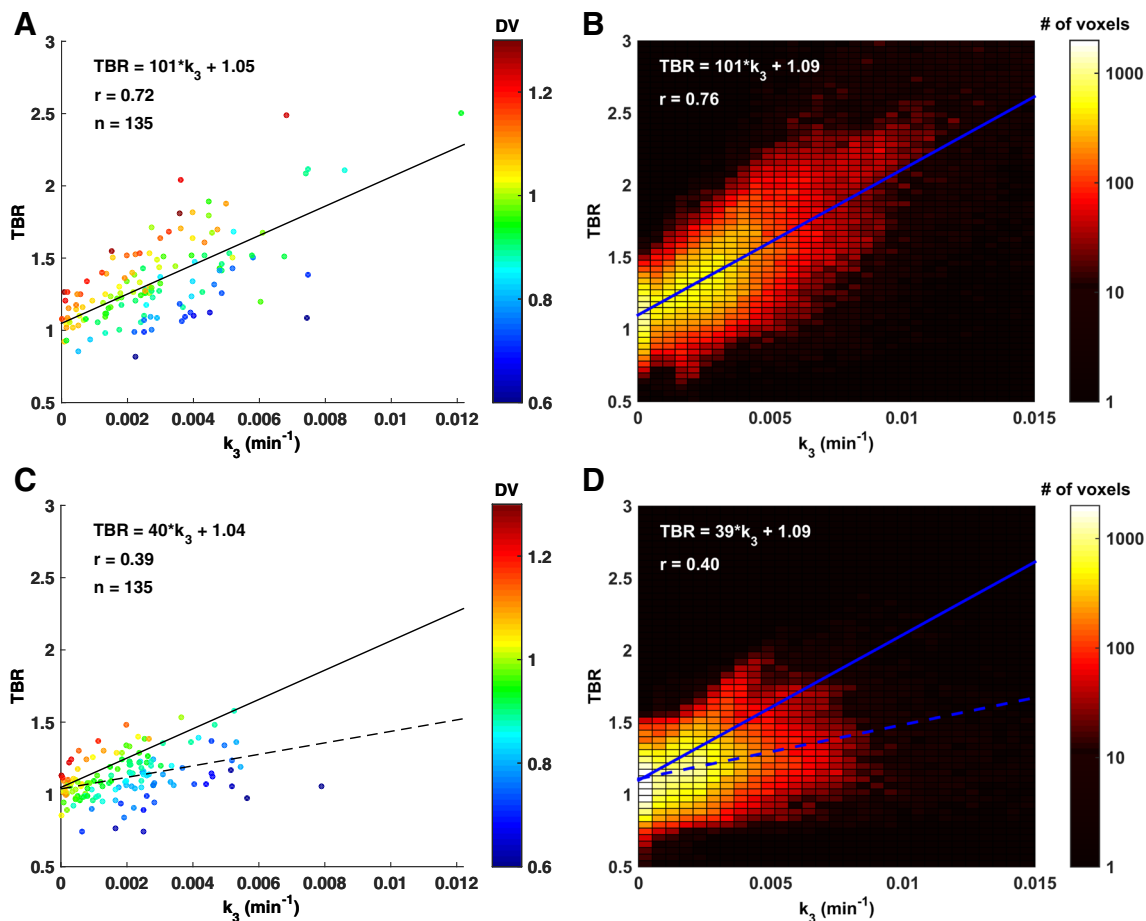


Fig. 3 Correlation between k_3 and TBR as derived from baseline and early response FMISO dynamic PET scans. **a** Scatterplot (one point per patient tumor) of the mean intratumor k_3 versus TBR at baseline, with linear regression fit (solid line). The points are color-coded according to the magnitude of the mean intratumor DV at baseline. **b** k_3 - TBR intensity histogram consisting of the pooled voxels from all tumors from baseline

data, with the linear regression fit (solid line). **c** Scatterplot of mean intratumor k_3 and TBR from early response scans, with included linear regression fit (dashed line). Superimposed is the linear regression fit from baseline data (**a**; solid line). **d** Corresponding intensity histogram from early response scans, with included linear regression fit (dashed line). Superimposed is the linear regression fit from baseline data (**b**; solid line)

changes that might be helpful in identifying appropriate therapeutic options. However, the added benefit of performing FMISO dPET depends on the clinical task. For example, in a clinical trial where absence of hypoxia in both primaries and lymph nodes would lead to de-escalation of therapy [6], the disagreement regarding hypoxic status of lesions between visual analysis ($TMR > 1.2$) and pharmacokinetic modeling results ($k_3 \geq 0.0026 \text{ min}^{-1}$) would have affected 13 out of 72 patients; however, all of these patients exhibited lesions with $TMR = 1.2$ (i.e., if $TMR \geq 1.2$ were adopted as hypoxia threshold, there would be no disagreement between results from pharmacokinetic modeling and visual analysis for the purpose of dose de-escalation). Low DV values in these cases indicate the onset of therapy-induced necrosis, making such discordance possibly clinically inconsequential. The consequence of false positive hypoxia readings, i.e., when the nuclear medicine physician reports a $TMR > 1.2$ but the k_3 value is near zero, is less egregious (five out of 72

patients, Table 4). In such cases, dose de-escalation would not be recommended and conventional radiation therapy doses delivered. If hypoxia would have been targeted (e.g., via dose escalation), a consensus among the investigators would have to be reached on whether to classify patients as having hypoxic or normoxic lesions. However, the encouraging outcome results suggest that dose escalation, with the intent to improve outcome, is of lower priority in this cohort of patients. ^{18}F -FMISO pharmacokinetic modeling might be more useful for characterization of the response to treatments that have a direct effect on tumor vascularization and perfusion [29].

Further work is necessary to understand the clinical relevance of the disagreement between visual analysis and pharmacokinetic modeling results and to establish the reproducibility of pharmacokinetic modeling. As only four out of 72 patients were deceased at the time of writing (one metastatic recurrence, one local and metastatic recurrence and two deaths

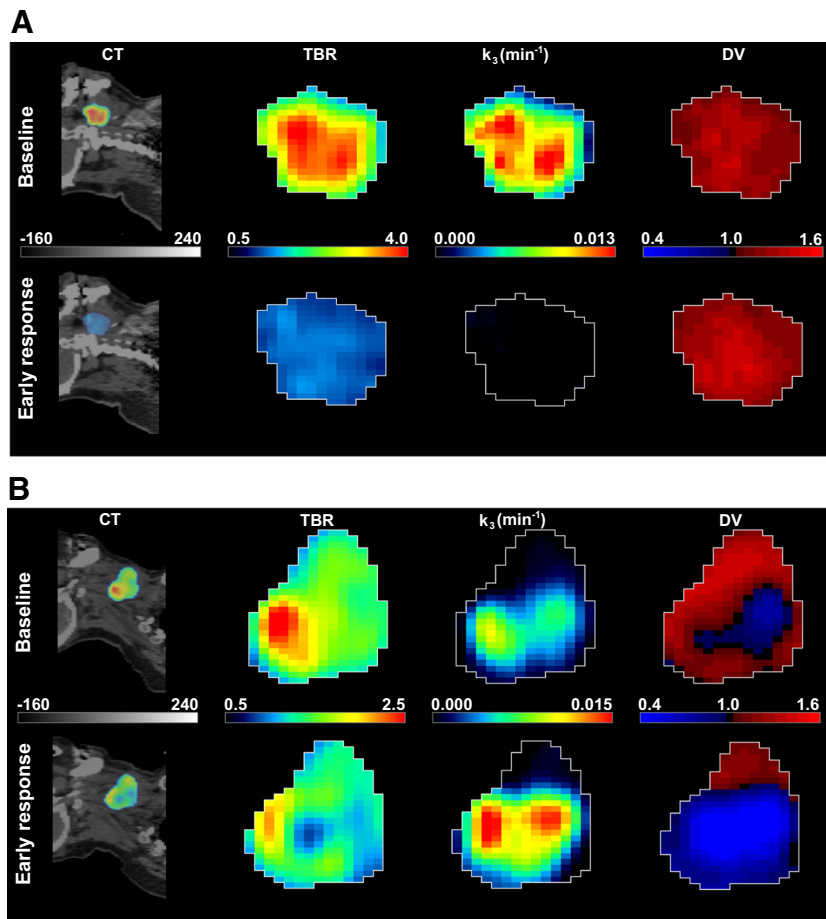


Fig. 4 Example of concordant and discordant changes in k_3 and TBR . **a** Patient #1 with 37 cm^3 T4aN2c, HPV-positive, p16-positive tumor originating in the tonsil. Results from baseline and early response scans are presented in top and bottom rows, respectively. From left to right: Sagittal view of the late 10-min FMISO PET/CT scan, tumor-to-blood ratio (TBR) map of intratumor voxels, k_3 map representing hypoxia-mediated entrapment of FMISO and FMISO distribution volume (DV), representing overall concentration of unbound FMISO relative to blood. For this patient,

both TBR and k_3 decreased after 1 cycle of chemoradiotherapy, while DV did not change substantially. $\Delta TBR = -1.26$ ($\Delta TBR_{max} = -2.82$), $\Delta k_3 = -0.0066 \text{ min}^{-1}$ ($\Delta k_{3,max} = -0.0160 \text{ min}^{-1}$), $\Delta DV = -0.01$. **b** Corresponding images for Patient #2 with 44 cm^3 T1N2b, HPV-negative, p16-negative tumor originating in the supraglottic larynx. For this patient, TBR decreased, while k_3 increased. Decreased DV further contributed to underestimation of TBR . $\Delta TBR = -0.17$ ($\Delta TBR_{max} = -0.71$), $\Delta k_3 = 0.0026 \text{ min}^{-1}$ ($\Delta k_{3,max} = 0.0059 \text{ min}^{-1}$), $\Delta DV = -0.24$

from other causes; median follow-up period: 26 months), and an additional two patients experienced local recurrence,

survival analysis is presently underpowered due to a paucity of events.

Table 4 Discordance between visual analysis and pharmacokinetic modeling for identification of patients with hypoxia ($n = 72$ patients)

	Baseline	Early response
Patients with no hypoxic lesions according to $TMR > 1.2$ (VA-)	3	23
Patients with no hypoxic lesions according to $k_3 > 0.0026 \text{ min}^{-1}$ (PM-)	4	15
VA-, PM-	1	10
VA-, PM+	2	13
VA+, PM+	66	44
VA+, PM-	3	5

TMR - Tumor-to-Muscle Ratio, VA - visual analysis, PM - pharmacokinetic modeling

Conclusion

Pharmacokinetic modeling of FMISO dynamic PET reveals a more detailed characterization of the tumor microenvironment and assessment of response to chemoradiotherapy in HNC patients than a single static image does. In a clinical trial where absence of hypoxia in primary tumor and lymph nodes would lead to de-escalation of therapy, the observed disagreement between visual analysis and pharmacokinetic modeling results would have affected patient management in <20% cases. While simple static PET imaging is easily implemented for clinical trials, the

clinical applicability of pharmacokinetic modeling remains to be investigated.

Compliance with ethical standards

Funding This study was supported by NIH grants 5R01CA157770–04 (P.I. Nancy Y. Lee), U01 CA157442–3 (P.I. Sadek A. Nehmeh) and the Cancer Center grant P30 CA008748 (P.I. Craig B. Thompson).

Conflict of interest The authors declare no potential conflicts of interest.

Ethical approval All procedures performed in studies involving human participants were in accordance with the ethical standards of the institutional and/or national research committee and with the 1964 Helsinki Declaration and its later amendments or comparable ethical standards.

Informed consent Informed consent was obtained from all individual participants included in the study.

References

- Schöder H, Fury M, Lee N, Kraus D. PET monitoring of therapy response in head and neck squamous cell carcinoma. *J Nucl Med*. 2009;50(Suppl 1):74S–88S.
- Moding EJ, Kastan MB, Kirsch DG. Strategies for optimizing the response of cancer and normal tissue to radiation. *Nat Rev Drug Discov*. 2013;12:526–42.
- Dubois LJ, Niemans R, van Kuijk SK, et al. New ways to image and target tumour hypoxia and its molecular responses. *Radiother Oncol*. 2015;116:352–7.
- van Dijk LK, Boerman OC, Kaanders JH, Bussink J. PET imaging in head and neck cancer patients to monitor treatment response: a future role for EGFR-targeted imaging. *Clin Cancer Res*. 2015;21:3602–9.
- Yankeelov TE, Mankoff DA, Schwartz LH, et al. Quantitative imaging in cancer clinical trials. *Clin Cancer Res*. 2016;22:284–90.
- Lee NY, Schöder H, Beattie B, et al. Strategy of using intratreatment hypoxia imaging to selectively and safely guide radiation dose de-escalation concurrent with chemotherapy for Locoregionally advanced human papillomavirus-related oropharyngeal carcinoma. *Int J Radiat Oncol Biol Phys*. 2016;96:9–17.
- Yeh JJ, Kim WY. Targeting tumor hypoxia with hypoxia-activated prodrugs. *J Clin Oncol*. 2015;33:1505–8.
- Padhani AR, Miles KA. Multiparametric imaging of tumor response to therapy. *Radiology*. 2010;2:348–64.
- Sharma RA, Plummer R, Stock JK, et al. Clinical development of new drug-radiotherapy combinations. *Nat Rev Clin Oncol*. 2016;13:627–42.
- Horsman MR, Mortensen LS, Petersen JB, Busk M, Overgaard J. Imaging hypoxia to improve radiotherapy outcome. *Nat Rev Clin Oncol*. 2012;9:674–87.
- Overgaard J. Hypoxic modification of radiotherapy in squamous cell carcinoma of the head and neck—a systematic review and meta-analysis. *Radiother Oncol*. 2011;100:22–32.
- Lim AM, Rischin D, Fisher R, et al. Prognostic significance of plasma osteopontin in patients with locoregionally advanced head and neck squamous cell carcinoma treated on TROG 02.02 phase III trial. *Clin Cancer Res*. 2012;18:301–7.
- DiSilvestro PA, Ali S, Craighead PS, et al. Phase III randomized trial of weekly cisplatin and irradiation versus cisplatin and tirapazamine and irradiation in stages IB2, IIA, IIB, IIIB, and IVA cervical carcinoma limited to the pelvis: a gynecologic oncology group study. *J Clin Oncol*. 2014;32:458–64.
- Koh WJ, Rasey JS, Evans ML, et al. Imaging of hypoxia in human tumors with [F-18]fluoromisonidazole. *Int J Radiat Oncol Biol Phys*. 1992;22:199–212.
- Rasey JS, Koh WJ, Evans ML, et al. Quantifying regional hypoxia in human tumors with positron emission tomography of [18F]fluoromisonidazole: a pretherapy study of 37 patients. *Int J Radiat Oncol Biol Phys*. 1996;36:417–28.
- Okamoto S, Shiga T, Yasuda K, et al. High reproducibility of tumor hypoxia evaluated by 18F-fluoromisonidazole PET for head and neck cancer. *J Nucl Med*. 2013;54:201–7.
- Grkovski M, Schwartz J, Rimmer A, et al. Reproducibility of 18F-fluoromisonidazole intratumour distribution in non-small cell lung cancer. *EJNMMI Res*. 2016;6:79.
- Grkovski M, Schöder H, Lee NY, et al. Multiparametric imaging of tumor hypoxia and perfusion with 18F-fluoromisonidazole dynamic PET in head and neck cancer. *J Nucl Med*. 2017; doi:10.2967/jnumed.116.188649.
- Koch CJ, Evans SM. Optimizing hypoxia detection and treatment strategies. *Semin Nucl Med*. 2015;45:163–76.
- Rajendran JG, Mankoff DA. Positron emission tomography imaging of blood flow and hypoxia in tumors. In: Shields AF, Price P (eds) *In vivo imaging of cancer therapy*. Springer Science & Business Media, 2007.
- Kadmas DJ, Hoffman JM. Methodology for quantitative rapid multi-tracer PET tumor characterizations. *Theranostics*. 2013;3:757–73.
- Dunnwald LK, Gralow JR, Ellis GK, Livingston RB, Linden HM, Specht JM, et al. Tumor metabolism and blood flow changes by positron emission tomography: relation to survival in patients treated with neoadjuvant chemotherapy for locally advanced breast cancer. *J Clin Oncol*. 2008;26:4449–57.
- Komar G, Kauhanen S, Liukko K, Seppänen M, Kajander S, Ovaska J, et al. Decreased blood flow with increased metabolic activity: a novel sign of pancreatic tumor aggressiveness. *Clin Cancer Res*. 2009;15:5511–7.
- Zips D, Zöphel K, Abolmaali N, et al. Exploratory prospective trial of hypoxia-specific PET imaging during radiochemotherapy in patients with locally advanced head-and-neck cancer. *Radiother Oncol*. 2012;105:21–8.
- Wiedenmann NE, Bucher S, Hentschel M, et al. Serial [18F]-fluoromisonidazole PET during radiochemotherapy for locally advanced head and neck cancer and its correlation with outcome. *Radiother Oncol*. 2015;117:113–7.
- Barcellos-Hoff MH, Park C, Wright EG. Radiation and the micro-environment - tumorigenesis and therapy. *Nat Rev Cancer*. 2005;5:867–75.
- Dewhirst MW, Cao Y, Moeller B. Cycling hypoxia and free radicals regulate angiogenesis and radiotherapy response. *Nat Rev Cancer*. 2008;8:425–37.
- Paudyal R, Oh JH, Riaz N, et al. Intravoxel incoherent motion diffusion-weighted MRI during chemoradiation therapy to characterize and monitor treatment response in human papillomavirus head and neck squamous cell carcinoma. *J Magn Reson Imaging*. 2017;45:1013–23.
- Grkovski M, Emmas SA, Carlin SD. 18F-fluoromisonidazole kinetic modeling for characterization of tumor perfusion and hypoxia in response to antiangiogenic therapy. *J Nucl Med*. 2017; doi:10.2967/jnumed.117.190892.